Desalination and Water Treatment
www.deswater.com

doi: 10.5004/dwt.2021.26861

212 (2021) 452–461
February

Adsorption of Direct Red 243 dye onto clay: kinetic study and isotherm analysis

Erbil Kavcı

Faculty of Engineering and Architecture, Department of Chemical Engineering, Kafkas University, Kars 36100, Turkey, email: erbilkavci@gmail.com

Received 13 April 2020; Accepted 28 November 2020

ABSTRACT

In this study, the adsorption of Direct Red 243 dye on clay was investigated in aqueous solutions. In batch adsorption experiments, the effects of initial pH, adsorbent dose, initial concentration, contact time, and temperature were investigated. X-ray diffraction, Fourier transform infrared spectroscopy, and surface area (S_{BET}) analysis were used to determine the properties of the clay. Scanning electron microscopy images of the clay were obtained before and after the adsorption of the dye. The Langmuir, Freundlich, Temkin, and Dubinin–Radushkevich isotherms were applied to the adsorption equilibrium, and the results indicated that the Langmuir isotherm gave the best fit to the data. The maximum adsorption capacity was 156.25 mg g^{-1} for Direct Red 243. The pseudo-first-order, pseudo-second-order, Elovich, and intra-particle diffusion models were applied to the data, and the kinetic data were best described by the pseudo-second-order model.

Keywords: Adsorption; Direct Red 243; Dyes; Clay; Isotherm; Kinetics

1. Introduction

Dyes are widely used in the textile, rubber, plastic, leather, cosmetic, pharmaceutical, and food industries. The use of dyes has also been increasing in these constantly developing and growing sectors [1]. Therefore, more wastewater containing dyes is discharged into the environment and the presence of dyes in wastewater is an important problem [2]. Worldwide, 700,000 tons of dye is produced annually, around 10%–15% of which is discharged into the environment. Dyes are visible in water bodies, even at a concentration of less than 1 ppm [3]. Annually 2.8×10^5 tons of textile dye is discharged into the environment [4]. Dyes discharged into the environment do not readily decompose because they are stable to sunlight as well as chemical and biological processes [5–7]. These toxic and carcinogenic dyes affect the entire ecosystem, from plants to animals and humans [8–11]. Since dyes can easily diffuse into the environment in which all life exists, it is important to remove them from wastewater [12–14].

Dyes are classified as acidic, basic, direct, reactive, disperse, and metal-complexed. Acidic, direct, and reactive dyes are anionic molecules [15]. Direct dyes contain one or more azo groups and are commonly used for coloring and printing cellulosic fibers [16,17]. Direct dyes have much higher molecular weights than other dyes and their adsorption mechanism involves the formation of hydrogen and Van der Waals bonds. Directs dyes are soluble in water because they contain sulfonate groups [18]. Most of the direct dyes contain azo groups and are toxic, carcinogenic, and mutagenic, causing dermatitis, skin irritation, and cancer. Azo dyes represent 60%–70% of all synthetic dyes. About 80% of dyes used in the dying process are azo dyes and need to be removed from wastewater [19,20].

Numerous biological, chemical, and physicochemical methods are used for the removal of dyes from wastewater, including flocculation, coagulation, precipitation, membrane filtration, electrochemical techniques, ozonation, photocatalytic degradation, and adsorption. The most suitable method is selected depending on the purpose and the

1944-3994/1944-3986

conditions [21–24]. Adsorption is the predominant method owing to its ease of application, low cost, minimal toxic waste, and high yield [25]. If the adsorbent used has a large surface area and is a readily available and low-cost material, the effectiveness of the adsorption is further increased, and clay is readily available and low-cost material.

The most common adsorbent is activated carbon but, owing to its high cost, it is preferable to use cheaper and more abundant materials. One of these alternative materials is clay [26–28]. Clay is a non-toxic hydrous aluminosilicate with fast adsorption kinetics and high adsorption capacity, as well as having complexation ability [29,30]. However, the adsorption capacity of clay in the removal of Direct Red 243 (DR243) dye has not been investigated.

In this study, clay was selected as the adsorbent since it is abundant and cheap. DR243 which is azo dyes was selected as the adsorbate because it is widely used in the textile industry. The removal of DR243 dyes by clay was evaluated in aqueous solutions. The clay was characterized and the effects on the adsorption of the initial pH, amount of adsorbent, initial concentration, contact time, and temperature were investigated via batch kinetic experiments. The pseudo-first, pseudo-second, Elovich, and intra-particle diffusion kinetic models were subsequently investigated using the obtained data. Isotherm studies were performed to understand the adsorption system.

2. Materials and methods

2.1. Adsorbent

The clay was obtained from Kars Cement Factory (Kars/Turkey). First, the clay was washed with distilled water and dried at 105°C for 24 h. The chemical composition of the clay was obtained by Kars Cement Factory. Combination ratio of clay are shown in Table 1. A Bruker, VERTEX 70v (MA USA) was used to record the infrared spectrum of the clay in the range of 4,000–400 cm^{-1}. The specific surface area was measured using the Brunauer, Emmett, and Teller (BET) method. The physical properties of the clay are presented in Table 2. SEM images were obtained before and after adsorption (DAYTAM, Turkey).

2.2. Adsorbate

Direct Red 243 (DR243) was obtained from a textile factory in Turkey. The molecular weight of the dye is 1,116.91 g mol^{-1} and maximum wavelength of DR243 is 517 nm. The molecular structure of the DR243 dye is shown in Fig. 1. DR243 was used in the experiments without any purification. Initially, a 1,000 mg L^{-1} stock solution was prepared by dissolving the dye in pure water. Other concentrations used in the experiments were obtained by dilution of this solution. The pH of the solution was adjusted by adding 0.1 mol L^{-1} HCl and NaOH solutions.

2.3. Adsorption studies

The effects of pH, adsorbent dose, initial concentration, contact time, and temperature on the adsorption of DR243 were investigated in batch experiments. Examining the effect of any parameter, the other parameter values were set as follows: amount of adsorbent: 2 g L^{-1}; temperature: 30°C; stirring speed: 180 rpm; initial concentration of the dye: 200 mg L^{-1}; pH: 2. After the adsorption experiments were completed, the samples were centrifuged at 5,000 rpm for 10 min and a UV-visible spectrophotometer (Mapada V1100D) was used to determine the dye concentration. The percentage dye adsorbed, the amount of dye at equilibrium time q_e (mg g^{-1}), and the amount of dye, q_t (mg g^{-1}), were calculated using Eqs. (1)–(3):

$$\%R = \frac{C_0 - C_e}{C_0} \times 100 \tag{1}$$

$$q_e = \frac{(C_0 - C_e) \times V}{m} \tag{2}$$

$$q_t = \frac{(C_0 - C_t) \times V}{m} \tag{3}$$

where C_0, C_e, and C_t (mg L^{-1}) represent the concentration of dye at the beginning, at equilibrium, and at any moment, respectively, V represents the volume of solution (L), and m represents the amount of adsorbent (g).

2.4. Adsorption isotherms

Isotherms are used to determine adsorption capacity and adsorbent–adsorbate behavior. The Langmuir, Freundlich, Temkin, and Dubinin–Radushkevich isotherms are widely applied to adsorption processes.

The linear equation of the Langmuir isotherm, which assumes that adsorption processes are monolayer, homogeneous, and have equal energies, is expressed as follows:

$$\frac{C_e}{q_e} = \frac{1}{q_{\max} K_L} + \frac{C_e}{q_{\max}} \tag{4}$$

Table 1
Chemical composition of clay

Content	Quantity %
SiO_2	53.86
Al_2O_3	13.76
CaO	11.12
Fe_2O_3	6.55
MgO	3.25
K_2O	1.59
Na_2O	0.96
SO_3	0.24
Cl	0.0875
LOI	8.58

Table 2
Physical properties of clay

BET surface area (m^2 g^{-1})	64.286
Average pore diameter (nm)	5.0098
Total pore volume (m^3 g^{-1})	0.080514

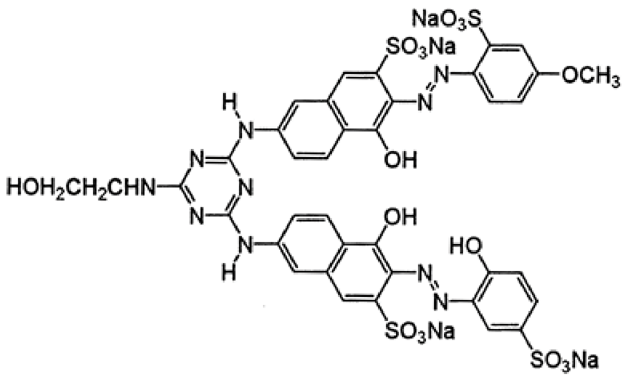

Fig. 1. Molecular structure of DR243 dye.

where q_{max} and K_L are calculated from the slope and intercept of the plot of C_e vs. C_e/q_e. The graph q_e of Langmuir isotherm corresponds to the amount of adsorbate per unit adsorbent mass at equilibrium (mg g^{-1}), q_{max} indicates the maximum adsorption capacity of the adsorbent (mg g^{-1}), C_e indicates the dye concentration (mg L^{-1}) in solution at equilibrium, and K_L is the Langmuir adsorption constant (L mg^{-1}) [31].

A characteristic value of the Langmuir isotherm, R_L, is calculated using the following equation:

$$R_L = \frac{1}{1 + K_L C_0} \tag{5}$$

where C_0 is the highest initial concentration of the dye (mg L^{-1}). If $R_L > 1$, the isotherm is not favorable whereas if $R_L = 1$, it is linear. A value of $0 < R_L < 1$ indicates that adsorption is favorable and $R_L = 0$ indicates that it is reversible.

The linear expression of the Freundlich isotherm [32], which states that the adsorption process is heterogeneous, is as follows:

$$\ln q_e = \ln K_F + \left(\frac{1}{n}\right)\ln C_e \tag{6}$$

where $1/n$ and K_F are calculated from the slope and intercept of the plot of $\ln(q_e)$ vs. $\ln(C_e)$ and K_F and n are the Freundlich constants.

The Temkin isotherm [33], which assumes a linear decrease in adsorption with temperature, is expressed in the following formula.

$$q_e = \frac{RT}{b_T}\ln A_T + \frac{RT}{b_T}\ln C_e \tag{7}$$

where q_e is plotted against $\ln(C_e)$, the slope of the plot corresponds to A_T and the intercept is b_T. A_T (L g^{-1}) and b_T (J mol^{-1}) are the Temkin constants. T (K) is the absolute temperature and R is the universal gas constant (8.314 J mol^{-1} K^{-1}).

The Dubinin–Raduskevich isotherm explains the relationship between the adsorbate and the adsorption mechanism [34]. It is expressed as follows:

$$\ln(q_e) = \ln(q_m) - \beta\varepsilon^2 \tag{8}$$

where ε is the Polanyi potential and is calculated using $\varepsilon = RT\ln\left(1 + \frac{1}{C_e}\right)$.

where q_e is the amount of adsorbed dye per unit adsorbent (mol L^{-1}), q_m is the theoretical monolayer saturation capacity (mol g^{-1}), C_e is the concentration of dye in solution at equilibrium (mol L^{-1}), ε (mmol^2 kJ^{-2}), D–R is the adsorption energy constant, R is the gas constant (8,314 kJ mol^{-1} K^{-1}), T is the temperature (K). $E = \frac{1}{\sqrt{2\beta}}$ (kJ mol^{-1}) and the magnitude of E is used to determine the adsorption mechanism. If E is less than 8 kJ mol^{-1}, the adsorption process is physical. If E is between 8 and 16 kJ mol^{-1}, the adsorption process is ion-exchange. If E is in the range of 20 to 40 kJ mol^{-1}, the adsorption process is chemisorption [35].

2.5. Adsorption kinetics

The pseudo-first-order, pseudo-second-order, Elovich, and intra-particle diffusion kinetic models were used to determine the mechanisms controlling the adsorption process.

The pseudo-first-order kinetic model is:

$$\log(q_e - q_t) = \log q_e - \frac{k_1 t}{2.303} \tag{9}$$

where the rate constant (k_1) is calculated from the slope of the plot of $\log(q_e - q_t)$ and t [28].

q_e and q_t are the equilibrium and adsorption capacities (mg g^{-1}) at time t, k_1 is the pseudo-first-order constant (min^{-1}), and t is the contact time.

The pseudo-second-order model is:

$$\frac{t}{q_t} = \frac{1}{k_2 q_e^2} + \frac{1}{q_e t} \tag{10}$$

where q_e is calculated from the slope of the plot of t against t/q_t. The second-order rate constant (k_2) (g mg^{-1} min^{-1}) is calculated from the intercept [36].

The Elovich model [37] is:

$$q_t = \frac{1}{\beta}\ln(\alpha\beta) + \frac{1}{\beta}\ln(t) \tag{11}$$

where (1/β) and 1/β ln(αβ) are calculated from the slope and intercept, respectively, of the plot of q_t against ln(t) where α is the initial adsorption rate (mg g^{-1} min$^{-0.5}$) and β is the desorption constant (g mg^{-1}).

The mathematical expression of this model is given below:

$$q_t = k_{id} t^{0.5} + C \tag{12}$$

where C and the diffusion rate constant (k_{id}) (mg g^{-1} min$^{-0.5}$) are calculated from the intercept and the slope of the plot of q_t vs. $t^{0.5}$ [38].

C is a value related to the thickness of the boundary layer. The greater the value of C, the greater the contribution of surface adsorption in the rate-controlling step. If the graph passes through the origin, it means that the step controlling the velocity fits the intra-particle diffusion model, and if it does not pass through the origin, it does not fit the intra-particle diffusion model [39].

3. Results and discussion

3.1. Characterization of the adsorbent

The composition of the clay was determined by X-ray diffraction (XRD) using a PANalytical EMPREYAN diffractometer with Cu Kα radiation. The predominant peaks found in the clay are shown in Fig. 2. The XRD pattern shows that the main components are calcium iron silicate and cristobalite, as well as kaolinite and ilvaite.

The FT-IR spectra of the clay before and after adsorption are presented in Fig. 3. The band detected at 3,620 cm^{-1} was attributed to the stretching vibrations of the hydroxyl group of Al–Al–OH. The band at about 1,620 cm^{-1} was caused by the stretching vibrations of C=C bonds [7]. The band at 1,440 cm^{-1} indicated the presence of C–O vibrations. The band at around 1,000 cm^{-1} was assigned to the symmetric stretching vibrations of Si–O–Si [2]. The band at 800 cm^{-1} was attributed to the Si–O bending of quartz [40]. The bands between 750 and 580 cm^{-1} were attributed to Al–O and Si–O deformations while the band at 520 cm^{-1} was assigned to Al–O–Si deformation. The FT-IR spectrum for the clay loaded with DR243 showed that the chemical nature of the clay remained virtually unchanged after DR243 adsorption. Therefore, the adsorption of DR243 onto clay was physical in nature.

The SEM surface images of the clay before and after adsorption are shown in Fig. 4. It was observed that the surface of the clay consisted of pores and flakes before adsorption, as indicated in Fig. 4a, which appeared to be filled with dye, as shown in Fig. 4b.

3.2. Effect of initial pH

One of the most important factors affecting dye adsorption is the initial pH. It affects the surface charge of the adsorbent and the dissociation of functional groups in active sites. In addition, the properties of the clay and the dye determine if a basic or acidic environment would be more favorable for the adsorption [41,42]. In this study, the behavior of the DR243 dye in the pH range from 2 to 9 is shown in Fig. 5. As can be seen from Fig. 5, the pH is highly effective for the adsorption of DR243 dye on clay. Approximately 84.5% of the dye is adsorbed at pH 2, while the amount of dye adsorbed decreases with increasing pH and no adsorption occurred above pH 6.

SiO_2, Al_2O_3, and CaO are the major constituents in the clay. As the pH decreases, the concentration of H^+ ions in the medium increases and negatively charged SiO_2 is balanced with hydrogen ions. At the same time, the positively charged components, Al_2O_3, and CaO, interact electrostatically with the negatively charged DR243 dye, allowed the dye to cling to the surface and favoring the adsorption [43,44]. With increasing pH, the concentration of OH^- ions increases and the sites on the adsorbent become negatively charged [45,46]. In this case, the repulsion forces are predominant between the clay and the DR243 dye. In addition, owing to the excess of OH^- ions in the solution, DR243 dye and OH^- ions compete with each other for the adsorbent and the rate of adsorption slows down [47,48]. Therefore, the following experiments were carried out at pH 2.

3.3. Adsorbent dose

To test the effect of the amount of adsorbent, varying amounts of clay adsorbent (0.05–0.5 g) were added to 50 mL of 200 mg L^{-1} DR243 solution. As shown in Fig. 6, the percentage of the dye adsorbed reached 95% at 0.2 g above which no further increase in adsorption was observed. However, the amount of dye adsorbed per gram of clay decreased from 129.7 to 18.83 mg g^{-1}.

3.4. Effect of initial concentration and contact time

The adsorption process was carried out with dye concentrations ranging from 100 to 300 mg L^{-1}. The effects of the initial concentration and contact time are shown in

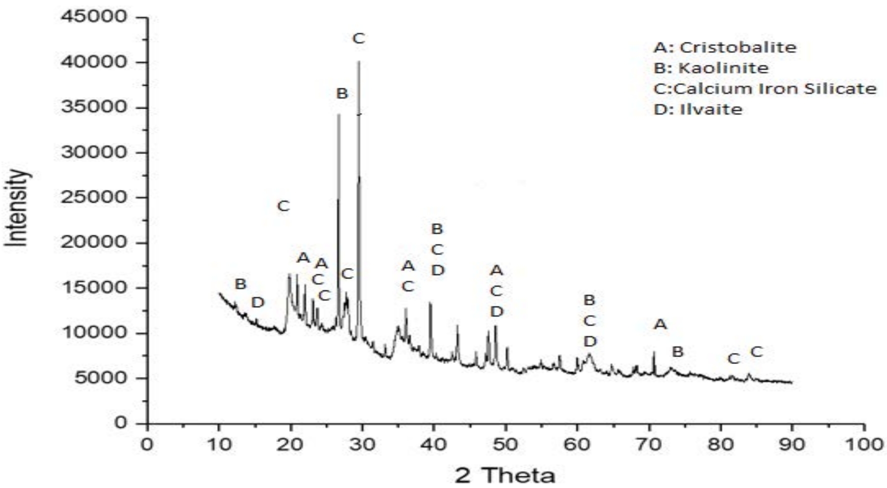

Fig. 2. XRD pattern for clay.

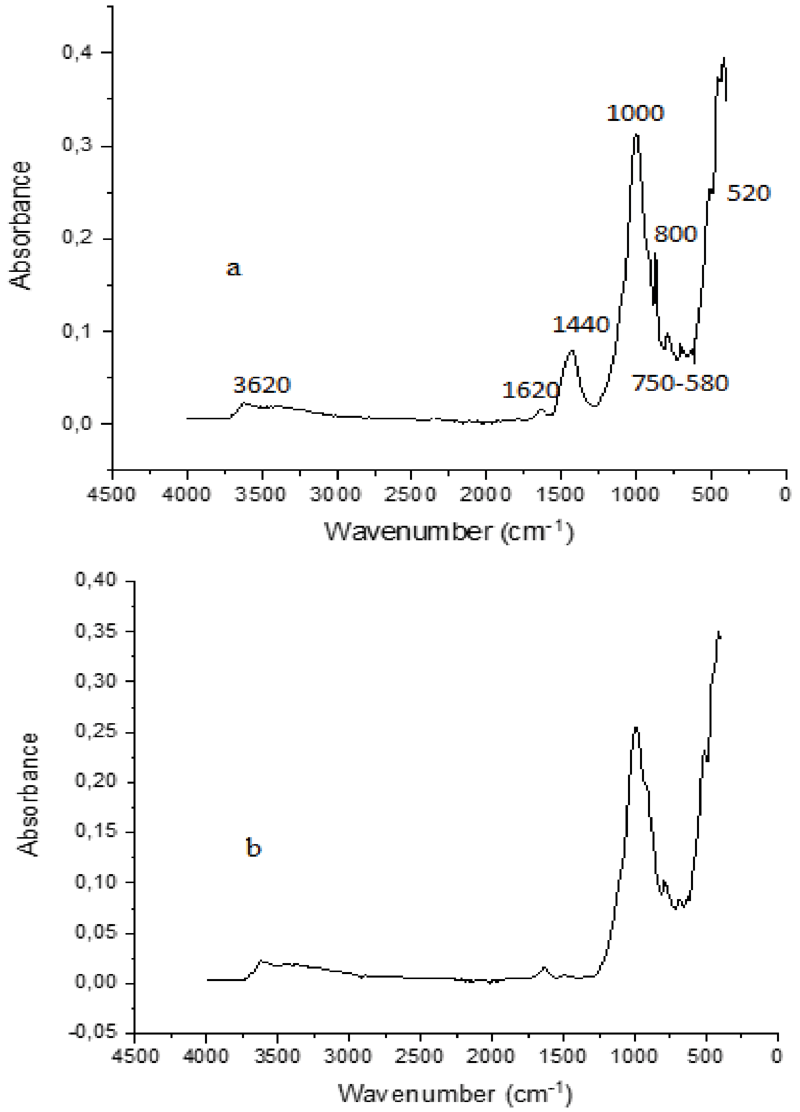

Fig. 3. FT-IR spectra for clay (a) before and (b) after adsorption.

Fig. 7. As the dye concentration increased, the amount of dye adsorbed increased. As the concentration difference increases at the interface between the dye solution and the adsorbent surface, the driving force leading to mass transfer increases further. As the dye concentration decreases, there are more available active sites on the adsorbent so the dye molecules can quickly and easily reach the active sites [49]. At all the concentrations examined, adsorption was very rapid in the first 5 min and then the amount of adsorbed dye started to decrease gradually. From 30 to 60 min, there was very little change in the percentage dye adsorbed until complete adsorption at the 60th minute. Thus, the equilibrium time is 60 min.

3.5. Effect of temperature

In the adsorption experiments performed at 22.5°C, 40°C, and 50°C, it was observed that the adsorption capacity of the clay decreases with increasing temperature. A decrease in the adsorption capacity with an increase in temperature indicates that the process is exothermic [50]. The attraction bond between the dye molecules and the active sites of the adsorbent weakens as the temperature increases so the amount of dye adsorbed decreases [51–53]. At different temperatures, the amount of DR243 dye adsorbed on clay was found to be: 94.24 mg g^{-1} at 22.5°C, 89.36 mg g^{-1} at 40°C, and 82.52 mg g^{-1} at 50°C. The results are presented graphically in Fig. 8.

3.6. Adsorption isotherms

The graphs for all the studied isotherms are shown in Fig. 9 and the constants and correlation coefficients calculated from these graphs are presented and compared in Table 3.

The Langmuir plot of C_e vs. C_e/q_e is shown in Fig. 9. The Langmuir isotherm showed the best fit with the experimental data (R^2 = 0.9918). The adsorption capacity

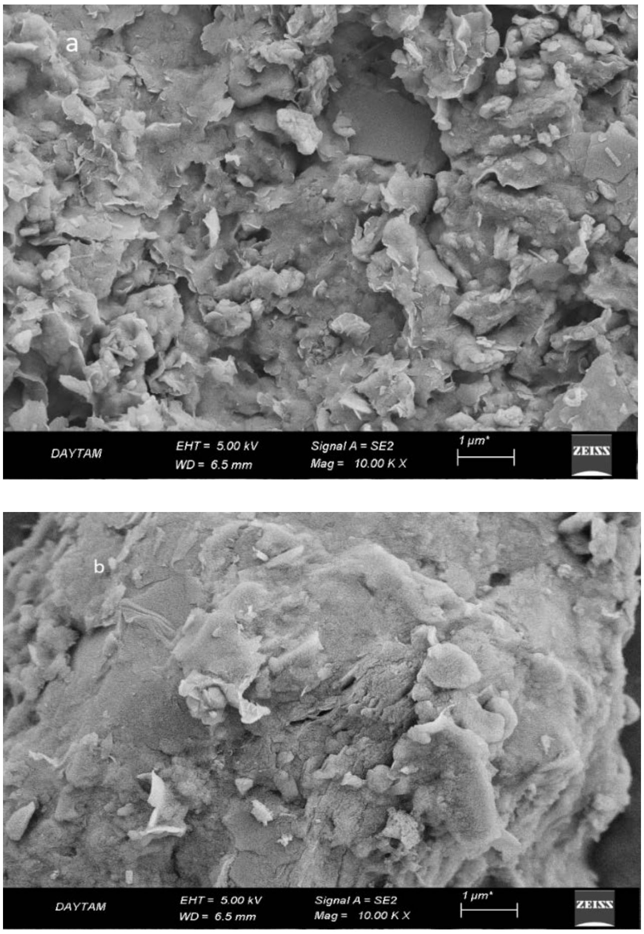

Fig. 4. SEM images of clay (a) before and (b) after adsorption.

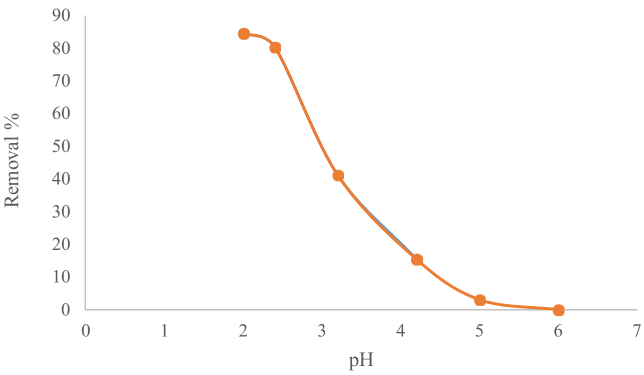

Fig. 5. Effect of initial pH on adsorption (C_0 = 200 mg L^{-1}; 180 rpm; 0.1 g; 30°C).

at 30°C was 156.25 mg g^{-1}, the R_L value was 0.67, and the adsorption was found to be favorable. For the Freundlich isotherm, the value of n was calculated from the graph of lnC_e vs. lnq_e, as shown in Fig. 9, and was greater than 1, which means that the adsorption was favorable, and the adsorption capacity was 18.83 mg g^{-1} (R^2 = 0.9819). The values A_T and b_T were calculated using Fig. 9 and Eq. (7). A_T was found to be 0.458 L g^{-1}, indicating adsorbate–adsorbent

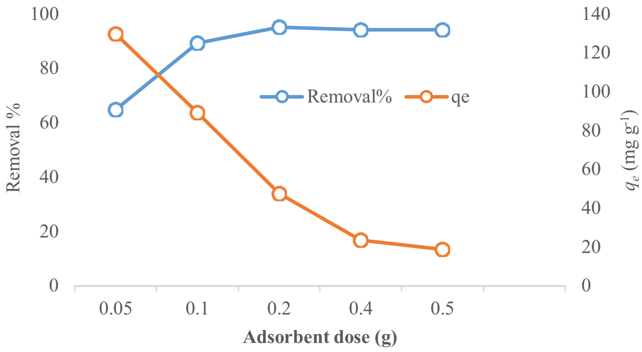

Fig. 6. Effect of adsorbent dose (C_0 = 200 mg L^{-1}; 180 rpm; pH = 2; 30°C).

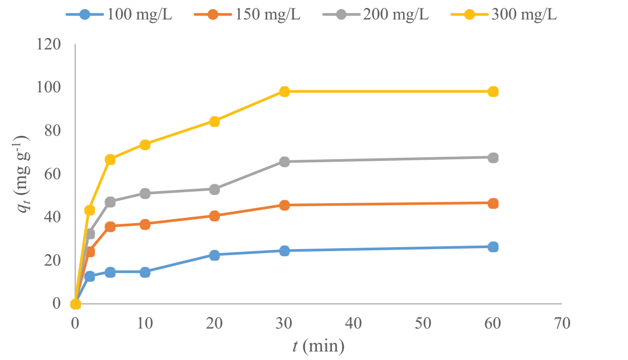

Fig. 7. Effect of initial concentration of the dye (0.2 g; 180 rpm; pH = 2; 30°C).

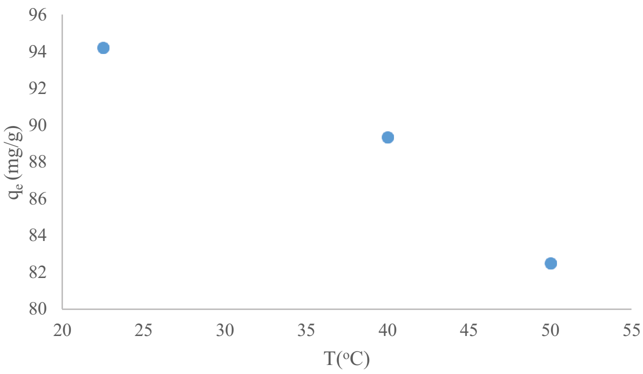

Fig. 8. Effect of temperature.

interactions. The value of b_T was 0.0723 kJ mol^{-1}, which is less than 8 kJ mol^{-1}, indicating that the adsorption process was physical for Temkin isotherm (R^2 = 0.9664). The D–R isotherm plot is given in Fig. 9. The E-value was calculated to be 0.2672 kJ mol^{-1} for DR243 according to $E = \frac{1}{\sqrt{2\beta}}$, which is in the range for physical adsorption. The correlation coefficient of D–R isotherm was 0.7909, indicating a poor fit to the data.

Table 3 shows the isotherm model parameters for the adsorption of DR243 onto the clay. From the comparison

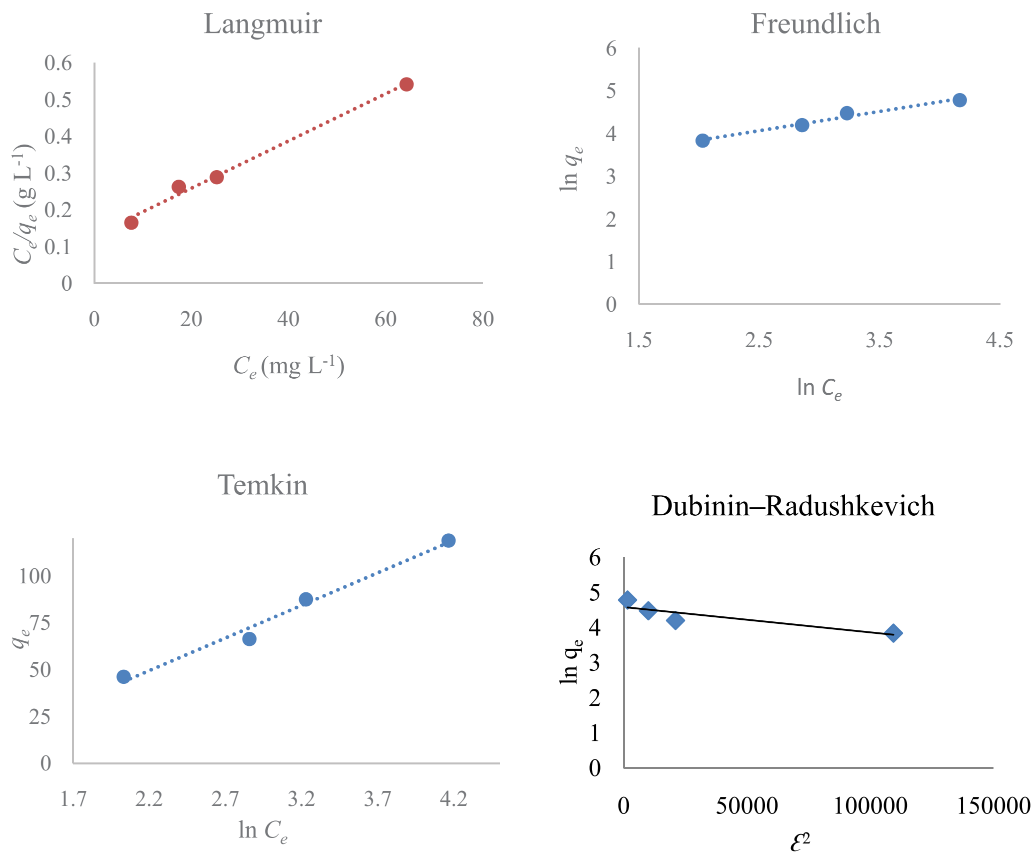

Fig. 9. Adsorption isotherms: (a) Langmuir, (b) Freundlich, (c) Temkin, and (d) Dubinin–Radushkevich isotherms.

Table 3
Constants of Langmuir, Freundlich, Temkin, and D–R isotherm models

Langmuir	q_{max} (mg g^{-1})	K_L	R_L	R^2
	156.25	0.0064	0.3828	0.9918
Freundlich	K_F	$1/n$		R^2
	18.83	0.4508		0.9819
Temkin	A_T (L g^{-1})	B	b_T (kJ mol^{-1} K^{-1})	R^2
	0.458	34.83	0.0723	0.9664
Dubinin–Radushkevich	q_m	E (kJ mol^{-1})		R^2
	4.5732	0.267261		0.7909

of correlation coefficients, the Langmuir isotherm model has showing that it best fits the experimental data and indicating that the adsorption process the highest R^2 value (0.9918). This means that the adsorption process is monolayer and homogenous and the sites have equal energies. The adsorption capacities of clay and other adsorbents for various anionic dyes are compared in Table 4.

3.7. Adsorption kinetics

The kinetic models are plotted in Fig. 10. The kinetic parameters from the pseudo-first-order, pseudo-second-order, Elovich, and intra-particle diffusion model are presented in Table 5.

The values of k_1 and k_2 were calculated from the plots of $\log(q_e - q_t)$ vs. t, and t/q_t vs. t, respectively, as shown in Fig. 10.

From comparison of the correlation coefficients (R^2) for all of the kinetic models in Table 4, the pseudo-second-order kinetic model shows the best fit with all correlation coefficients close to unity. Furthermore, the correlation coefficients for the pseudo-second-order kinetic model ($R^2 \geq 0.996$) were greater than those for the pseudo-first-order ($R^2 \leq 0.96$), and Elovich models ($R^2 \leq 0.96$). R^2 of Elovich is relatively low, indicating a chemical adsorption mechanism.

The values of k_i and C were obtained from the slope of the linear plot of q_t vs. $t^{0.5}$ from Fig. 10d. The intercept for this plot is not zero, meaning that intra-particle diffusion is not rate-limiting. The value of C (29.196–51.524 mg g^{-1})

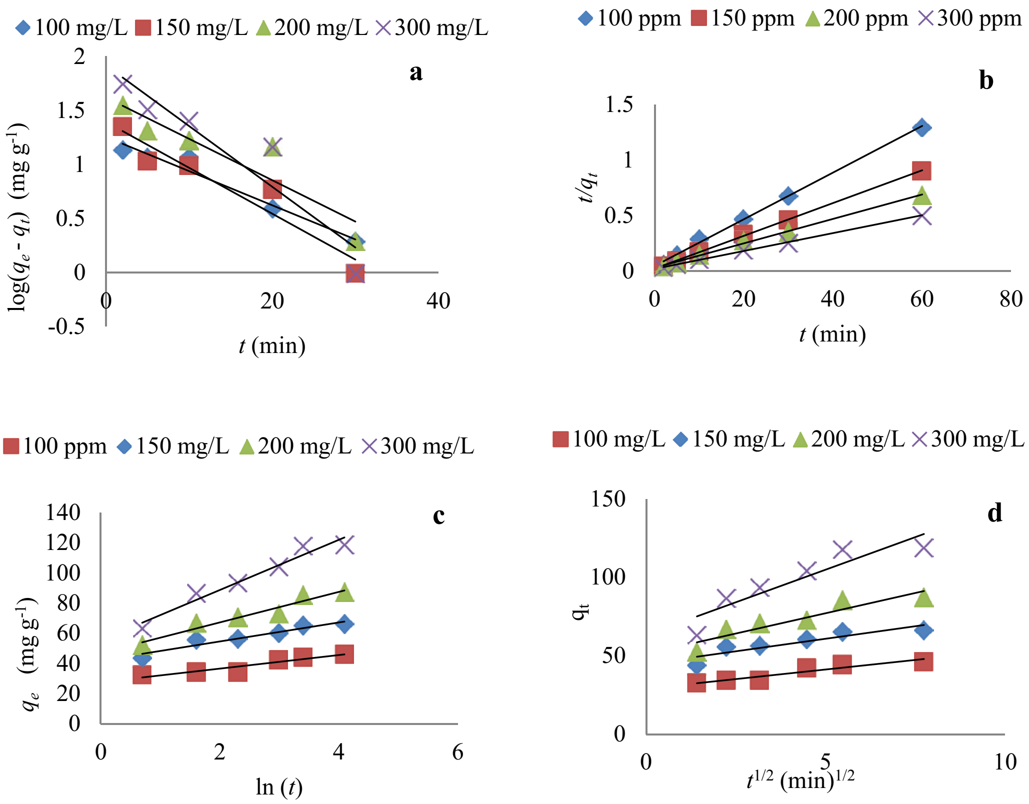

Fig. 10. Graphs of kinetic models: (a) pseudo-first-order, (b) pseudo-second-order, (c) Elovich, and (d) intra-particle diffusion.

Table 4
Adsorption capacities of different adsorbents for various anionic dyes

Adsorbent	Dye	q_{max} (mg g^{-1})	Isotherm/kinetics	References
Cattle hair waste	Acid Blue 161	104.787	Liu-general order	[54]
Spent tea leaves (modified polyethylemine)	Reactive Black 5	71.9	Temkin/pseudo-second-order	[55]
Turkish sepiolite	Reactive Blue 15	3.43	Freundlich/pseudo-second-order	[56]
Nerium oleander flower (activated carbon)	Direct turquoise blues	33.3	Langmuir and Freundlich/ pseudo-second-order	[57]
Cassava root husk	Direct Black ECO TFA	46.1	Langmuir/pseudo-second-order	[58]
Rice husk	Direct red 31/ Direct Orang 26	25.63/19.96	Langmuir/pseudo-second-order	[59]
Neam leaf powder	Congo Red	41.2	Langmuir/pseudo-second-order	[60]
Bentonite	Direct Red 2	153.84	Langmuir/pseudo-second-order	[61]
Palm ash	Direct Blue 71	400	Freundlich/pseudo-second-order	[62]
Sepiolite	Direct Blue 85	232	Langmuir/pseudo-first-order	[63]
Clay	Direct Red 243	156.25	Langmuir/pseudo-second-order	This study

increased with increasing initial concentration of dye. This means that the thickness of the boundary layer increased and that boundary layer diffusion is effective.

4. Conclusions

The adsorption of an anionic dye (DR243) onto clay was studied. Clay was characterized using XRD, FT-IR, and S_{BET}. The physical properties of clay show that it is suitable for use as a potential adsorbent. The results of the study indicated that pH was the most significant parameter affecting the adsorption process. As the pH decreased, the amount of adsorbed substance increased. The maximum adsorption capacity was obtained at pH 2 and no dye was adsorbed above pH 6. The adsorption process is exothermic as the amount adsorbed decreases with increasing

Table 5
Kinetic parameters

	Pseudo-first-order constants			Pseudo-second-order constants		
C_0 (mg L^{-1})	q_e (mg g^{-1})	k_1	R^2	q_e (mg g^{-1})	k_2	R^2
100	14.022	0.073005	0.9603	47.61905	0.009383	0.9981
150	24.79	0.097647	0.9125	68.02721	0.009562	0.9993
200	41.524	0.087975	0.8435	90.09009	0.004615	0.9966
300	82.243	0.129198	0.8841	123.4568	0.003216	0.9985
	Elovich constants			Intra-particle diffusion constants		
	α	β	R^2	k_{id}	C	R^2
100	2,212.06	0.223389	0.8917	2.4075	29.196	0.9014
150	4,579.89	0.156742	0.9291	3.1686	45.065	0.8009
200	1,100.93	0.099334	0.9348	5.1577	51.524	0.8575
300	464.176	0.060013	0.959	8.3515	51.524	0.842

temperature. The equilibrium time was found to be 60 min, which is relatively fast, so clay is feasible for use as an adsorbent. The experimental data was found to have the best fit to the Langmuir isotherm and the adsorption capacity of the clay was found to be 156.25 mg g^{-1}. The R_L value was less than 1, indicating that the adsorption was favorable. The adsorption of Direct Red 243 dye by clay fits the pseudo-second-order kinetic model. Owing to the low contact time and adsorbent dose required for adsorption of Direct Red 243 dye, and the relatively high adsorption capacity, clay can be used as an effective and low-cost adsorbent for the removal of Direct Red 243 dye from aqueous solutions.

References

[1] M.H. Karaoğlu, M. Doğan, M. Alkan, Kinetic analysis of reactive blue 221 adsorption on kaolinite, Desalination, 256 (2010) 154–165.

[2] J.E. Aguiar, J.A. Cecilia, P.A.S. Tavares, D.C.S. Azevedo, E.R. Castellón, S.M.P. Lucena, I.J. Silva, Adsorption study of reactive dyes onto porous clay heterostructures, Appl. Clay Sci., 135 (2017) 35–44.

[3] B. Shi, G. Li, D. Wang, C. Feng, H. Tang, Removal of direct dyes by coagulation: the performance of preformed polymeric aluminum species, J. Hazard. Mater., 143 (2007) 567–574.

[4] R.L. Singh, P.K. Singh, R.P. Singh, Enzymatic decolorization and degradation of azo dyes – a review, Int. Biodeterior. Biodegrad., 104 (2015) 21–31.

[5] M. Doğan, M.H. Karaoğlu, M. Alkan, Adsorption kinetics of maxilon yellow 4GL and maxilon red GRL dyes on kaolinite, J. Hazard. Mater., 165 (2009) 1142–1151.

[6] Ö. Gök, A.S. Özcan, A. Özcan, Adsorption behavior of a textile dye of Reactive Blue 19 from aqueous solutions onto modified bentonite, Appl. Surf. Sci., 256 (2010) 5439–5443.

[7] N. Liu, H. Wang, C.-H. Weng, C.-C. Hwang, Adsorption characteristics of Direct Red 23 azo dye onto powdered tourmaline, Arabian J. Chem., 11 (2018) 1281–1291.

[8] J. Erkmen, The use of hydroxyethyl cellulose as a transparent filling material in finishing polish, Pigm. Resin Technol., 47 (2018) 323–329, doi: 10.1108/PRT-06-2017-0060.

[9] A.T. Ojedokun, O.S. Bello, Kinetic modeling of liquid-phase adsorption of Congo red dye using guava leaf-based activated carbon, Appl. Water Sci., 7 (2017) 1965–1977.

[10] O. Bashir, M.N. Khan, T.A. Khan, Z. Khan, S.A. Al-Thabaiti, Influence of stabilizing agents on the microstructure of Co-nanoparticles for removal of Congo red, Environ. Technol. Innovation, 8 (2017) 327–342.

[11] T.A. Khan, M. Nazir, E.A. Khan, Magnetically modified multiwalled carbon nanotubes for the adsorption of bismarck brown R and Cd(II) from aqueous solution: batch and column studies, Desal. Water Treat., 57 (2016) 19374–19390.

[12] Z. Cheng, L. Zhang, X. Guo, X. Jiang, T. Li, Adsorption behavior of direct red 80 and congo red onto activated carbon/surfactant: process optimization, kinetics and equilibrium, Spectrochim. Acta, Part A, 137 (2015) 1126–1143.

[13] B.A. Fil, Isotherm, kinetic, and thermodynamic studies on the adsorption behavior of malachite green dye onto montmorillonite clay, Part. Sci. Technol., 34 (2016) 118–126.

[14] Z. Maderova, E. Baldikova, K. Pospiskova, I. Safarik, M. Safarikova, Removal of dyes by adsorption on magnetically modified activated sludge, Int. J. Environ. Sci. Technol., 13 (2016) 1653–1664.

[15] M. Asgher, Biosorption of Reactive Dyes: a review, Water Air Soil Pollut., 223 (2012) 2417–2435.

[16] E.S.Z. El Ashtoukhy, *Loofa egyptiaca* as a novel adsorbent for removal of direct blue dye from aqueous solution, J. Environ. Manage., 90 (2009) 2755–2761.

[17] X. He, M. Du, H. Li, T. Zhou, Removal of direct dyes from aqueous solution by oxidized starch cross-linked chitosan/silica hybrid membrane, Int. J. Biol. Macromol., 82 (2016) 174–181.

[18] A. Shams-Nateri, E. Dehnavi, E. Zahedi, PCA-spectroscopy study of common salt effect on solubility of direct dye, Pigm. Resin Technol., 46 (2017) 362–370.

[19] W. Konicki, M. Aleksandrzak, D. Moszyński, E. Mijowska, Adsorption of anionic azo-dyes from aqueous solutions onto graphene oxide: equilibrium, kinetic and thermodynamic studies, J. Colloid Interface Sci., 496 (2017) 188–200.

[20] S. Ziane, F. Bessaha, K. Marouf-Khelifa, A. Khelifa, Single and binary adsorption of reactive black 5 and Congo red on modified dolomite: performance and mechanism, J. Mol. Liq., 249 (2018) 1245–1253.

[21] N.N. Nassar, Kinetics, mechanistic, equilibrium, and thermodynamic studies on the adsorption of acid red dye from wastewater by γ-Fe_2O_3 nanoadsorbents, Sep. Sci. Technol., 45 (2010) 1092–1103.

[22] H. Wang, X. Yuan, G. Zeng, L. Leng, X. Peng, K. Liao, L. Peng, Z. Xiao, Removal of malachite green dye from wastewater by different organic acid-modified natural adsorbent: kinetics, equilibriums, mechanisms, practical application, and disposal of dye-loaded adsorbent, Environ. Sci. Pollut. Res., 21 (2014) 11552–11564.

[23] Z. Khan, O. Bashir, M.N. Khan, T.A. Khan, S.A. Al-Thabaiti, Cationic surfactant assisted morphology of Ag@Cu, and their

catalytic reductive degradation of Rhodamine B, J. Mol. Liq., 248 (2017) 1096–1108.
[24] M.N. Khan, O. Bashir, T.A. Khan, S.A. Al-Thabaiti, Z. Khan, CTAB capped synthesis of bio-conjugated silver nanoparticles and their enhanced catalytic activities, J. Mol. Liq., 258 (2018) 133–141.
[25] A. Xue, S. Zhou, Y. Zhao, X. Lu, P. Han, Adsorption of reactive dyes from aqueous solution by silylated palygorskite, Appl. Clay Sci., 48 (2010) 638–640.
[26] R. Ansari, Z. Mosayebzadeh, Removal of basic dye methylene blue from aqueous solutions using sawdust and sawdust coated with polypyrrole, J. Iran. Chem. Soc., 7 (2010) 339–350.
[27] E. Errais, J. Duplay, F. Darragi, Textile dye removal by natural clay – case study of Fouchana Tunisian clay, Environ. Technol., 31 (2010) 373–380.
[28] F.-C. Wu, R.-L. Tseng, R.-S. Juang, Kinetics of color removal by adsorption from water using activated clay, Environ. Technol., 22 (2001) 721–729.
[29] A.A. Adeyemo, I.O. Adeoye, O.S. Bello, Adsorption of dyes using different types of clay: a review, Appl. Water Sci., 7 (2017) 543–568.
[30] O. Lacin, A. Haghighatnia, F. Demir, F. Sevim, O. laçin, Adsorption characteristics and behaviors of natural red clay for removal of BY28 from aqueous solutions, Int. J. Trend Sci. Res. Dev., 3 (2019) 1037–1047.
[31] A.S. Özcan, Ş. Tetik, A. Özcan, Adsorption of acid dyes from aqueous solutions onto sepiolite, Sep. Sci. Technol., 39 (2005) 301–320.
[32] H.M.F. Freundlich, Over the adsorption in Solution, J. Phys. Chem., 57 (1906) 385–471.
[33] S.A. Sadat, A.M. Ghaedi, M. Panahimehr, M.M. Baneshi, A. Vafaei, M. Ansarizadeh, Rapid room-temperature synthesis of cadmium zeolitic imidazolate framework nanoparticles based on 1,1′-carbonyldiimidazole as ultra-high-efficiency adsorbent for ultrasound-assisted removal of malachite green dye, Appl. Surf. Sci., 467–468 (2019) 1204–1212.
[34] I.D. Mall, V.C. Srivastava, N.K. Agarwal, Removal of Orange-G and Methyl Violet dyes by adsorption onto bagasse fly ash—kinetic study and equilibrium isotherm analyses, Dyes Pigm., 69 (2006) 210–223.
[35] C.S.T. Araújo, I.L.S. Almeida, H.C. Rezende, S.M.L.O. Marcionilio, J.J.L. Léon, T.N. de Matos, Elucidation of mechanism involved in adsorption of Pb(II) onto lobeira fruit (*Solanum lycocarpum*) using Langmuir, Freundlich and Temkin isotherms, Microchem. J., 137 (2018) 348–354.
[36] L. Mouni, L. Belkhiri, J.-C. Bollinger, A. Bouzaza, A. Assadi, A. Tirri, F. Dahmoune, K. Madani, H. Remini, Removal of Methylene Blue from aqueous solutions by adsorption on Kaolin: kinetic and equilibrium studies, Appl. Clay Sci., 153 (2018) 38–45.
[37] F. Mashkoor, A. Nasar, Preparation, characterization and adsorption studies of the chemically modified *Luffa aegyptica* peel as a potential adsorbent for the removal of malachite green from aqueous solution, J. Mol. Liq., 274 (2019) 315–327.
[38] V. Vimonses, S. Lei, B. Jin, C.W.K. Chow, C. Saint, Kinetic study and equilibrium isotherm analysis of Congo Red adsorption by clay materials, Chem. Eng. J., 148 (2009) 354–364.
[39] M. Auta, B.H. Hameed, Acid modified local clay beads as effective low-cost adsorbent for dynamic adsorption of methylene blue, J. Ind. Eng. Chem., 19 (2013) 1153–1161.
[40] I. Chaari, E. Fakhfakh, M. Medhioub, F. Jamoussi, Comparative study on adsorption of cationic and anionic dyes by smectite rich natural clays, J. Mol. Struct., 1179 (2019) 672–677.
[41] N.K. Amin, Removal of direct blue-106 dye from aqueous solution using new activated carbons developed from pomegranate peel: adsorption equilibrium and kinetics, J. Hazard. Mater., 165 (2009) 52–62.
[42] A.M.M. Vargas, A.L. Cazetta, A.C. Martins, J.C.G. Moraes, E.E. Garcia, G.F. Gauze, W.F. Costa, V.C. Almeida, Kinetic and equilibrium studies: adsorption of food dyes Acid Yellow 6, Acid Yellow 23, and Acid Red 18 on activated carbon from flamboyant pods, Chem. Eng. J., 181–182 (2012) 243–250.
[43] E. Bulut, M. Özacar, İ.A. Şengil, Equilibrium and kinetic data and process design for adsorption of Congo Red onto bentonite, J. Hazard. Mater., 154 (2008) 613–622.
[44] I.D. Mall, V.C. Srivastava, N.K. Agarwal, I.M. Mishra, Adsorptive removal of malachite green dye from aqueous solution by bagasse fly ash and activated carbon-kinetic study and equilibrium isotherm analyses, Colloids Surf., A, 264 (2005) 17–28.
[45] M. Asif Tahir, H.N. Bhatti, M. Iqbal, Solar Red and Brittle Blue direct dyes adsorption onto *Eucalyptus angophoroides* bark: equilibrium, kinetics and thermodynamic studies, J. Environ. Chem. Eng., 4 (2016) 2431–2439.
[46] A. Özcan, Ç. Ömeroğlu, Y. Erdoğan, A.S. Özcan, Modification of bentonite with a cationic surfactant: an adsorption study of textile dye Reactive Blue 19, J. Hazard. Mater., 140 (2007) 173–179.
[47] I. Chaari, B. Moussi, F. Jamoussi, Interactions of the dye, C.I. direct orange 34 with natural clay, J. Alloys Compd., 647 (2015) 720–727.
[48] J. Huang, Y. Liu, Q. Jin, X. Wang, J. Yang, Adsorption studies of a water soluble dye, Reactive Red MF-3B, using sonication-surfactant-modified attapulgite clay, J. Hazard. Mater., 143 (2007) 541–548.
[49] T. Maneerung, J. Liew, Y. Dai, S. Kawi, C. Chong, C.-H. Wang, Activated carbon derived from carbon residue from biomass gasification and its application for dye adsorption: kinetics, isotherms and thermodynamic studies, Bioresour. Technol., 200 (2016) 350–359.
[50] M.-S. Chiou, H.-Y. Li, Equilibrium and kinetic modeling of adsorption of reactive dye on cross-linked chitosan beads, J. Hazard. Mater., 93 (2002) 233–248.
[51] Z. Aksu, S. Tezer, Biosorption of reactive dyes on the green alga *Chlorella vulgaris*, Process Biochem., 40 (2005) 1347–1361.
[52] O. Hamdaoui, Batch study of liquid-phase adsorption of methylene blue using cedar sawdust and crushed brick, J. Hazard. Mater., 135 (2006) 264–273.
[53] K.S. Thangamani, N. Muthulakshmi Andal, E. Ranjith Kumar, M. Saravanabhavan, Utilization of magnetic nano cobalt ferrite doped *Capra aegagrus* hircus dung activated carbon composite for the adsorption of anionic dyes, J. Environ. Chem. Eng., 5 (2017) 2820–2829.
[54] B. Mella, M.J. Puchana-Rosero, D.E.S. Costa, M. Gutterres, Utilization of tannery solid waste as an alternative biosorbent for acid dyes in wastewater treatment, J. Mol. Liq., 242 (2017) 137–145.
[55] S. Wong, H.H. Tumari, N. Ngadi, N.B. Mohamed, O. Hassan, R. Mat, N.A. Saidina Amin, Adsorption of anionic dyes on spent tea leaves modified with polyethyleneimine (PEI-STL), J. Cleaner Prod., 206 (2019) 394–406.
[56] A. Tabak, E. Eren, B. Afsin, B. Caglar, Determination of adsorptive properties of a Turkish Sepiolite for removal of Reactive Blue 15 anionic dye from aqueous solutions, J. Hazard. Mater., 161 (2009) 1087–1094.
[57] K. Durairaj, P. Senthilkumar, P. Velmurugan, S. Divyabharathi, D. Kavitha, Development of activated carbon from *Nerium oleander* flower and their rapid adsorption of direct and reactive dyes, Int. J. Green Energy, 16 (2019) 573–582.
[58] F.B. Scheufele, J. Staudt, M.H. Ueda, C. Ribeiro, V. Steffen, C.E. Borba, A.N. Módenes, A.D. Kroumov, Biosorption of direct black dye by cassava root husks: kinetics, equilibrium, thermodynamics and mechanism assessment, J. Environ. Chem. Eng., 8 (2020) 103533, doi: 10.1016/j.jece.2019.103533.
[59] Y. Safa, H.N. Bhatti, Kinetic and thermodynamic modeling for the removal of Direct Red-31 and Direct Orange-26 dyes from aqueous solutions by rice husk, Desalination, 272 (2011) 313–322.
[60] K.G. Bhattacharyya, A. Sharma, *Azadirachta indica* leaf powder as an effective biosorbent for dyes: a case study with aqueous Congo Red solutions, J. Environ. Manage., 71 (2004) 217–229.
[61] B. Zohra, K. Aicha, S. Fatima, B. Nourredine, D. Zoubir, Adsorption of Direct Red 2 on bentonite modified by cetyltrimethylammonium bromide, Chem. Eng. J., 136 (2008) 295–305.
[62] A.A. Ahmad, B.H. Hameed, N. Aziz, Adsorption of direct dye on palm ash: kinetic and equilibrium modeling, J. Hazard. Mater., 141 (2007) 70–76.
[63] S.C.R. Santos, R.A.R. Boaventura, Adsorption of cationic and anionic azo dyes on sepiolite clay: equilibrium and kinetic studies in batch mode, J. Environ. Chem. Eng., 4 (2016) 1473–1483.